On the hindlimb biomechanics of the avian take-off leap

3   E. A. Meilak[1,2], P. Provini[3], C. Palmer[2], N. J. Gostling[4,6], M. O. Heller[1,5,6]

4   1. Bioengineering Research Group, Faculty of Engineering and Physical Sciences, University of

5   Southampton, Southampton, UK; 2. Faculty of Environmental and Life Sciences, University of

6   Southampton, Southampton, UK; 3. Université de Paris, INSERM U1284, Center for Research and

7   Interdisciplinarity (CRI), F-75006 Paris, France; 4. School of Biological Sciences, Faculty of

8   Environmental and Life Sciences, University of Southampton, Southampton, UK; 5. Centre for Sport,

9   Exercise and Osteoarthritis Research Versus Arthritis, Southampton, UK; 6. Institute for Lifesciences,

10   University of Southampton, Southampton, UK

11   Correspondence:

12   Corresponding author

13   Prof. Dr.Markus O. Heller

14   University of Southampton

15   Faculty of Engineering and Physical Sciences

16   Department of Mechanical Engineering

17   Southampton

18   SO17 1BJ

19   United Kingdom

20   m.o.heller@soton.ac.uk

Abstract

Although extant land birds take to the air by leaping, generating the initial take-off velocity primarily from the hindlimbs, the detailed musculoskeletal mechanics remain largely unknown. We therefore simulated *in silico* the take-off leap of the zebra finch, *Taeniopygia guttata,* a model species of passerine, a class of bird which includes over half of all extant bird species. A 3D computational musculoskeletal model of the zebra finch hindlimb, comprising of 43 musculotendon units was developed and driven with previously published take-off ground reaction forces and kinematics. Using inverse dynamics, the external moments at the ankle, knee, and hip joints were calculated and contrasted to the cumulative muscle capability to balance these moments. Mean peak external flexion moments at the hip and ankle were 0.55 bodyweight times leg length (BWL) each whilst peak knee extension moments were about half that value (0.29 BWL). Muscles had the capacity to generate 146%, 230%, and 212 % of the mean peak external moments at the hip, knee, and ankle, respectively. Similarities in hindlimb morphology and external loading across passerine species suggest that the effective take-off strategy employed by the zebra finch may be shared across the passerine clade and therefore half of all birds.

Introduction

Take-off is a crucial part of avian flight, requiring energy-intensive motion to accelerate into the air. Understanding how birds make the transition from standing statically to being airborne is one of the key components necessary for understanding how avian flight evolved. Previous work on the take–off of a variety of land birds demonstrated that the hindlimb plays a major role in propelling the bird in to the air, and suggests that the bipedal leap generates approximately 80-90% of the take-off velocity [1-6]. The group Passeriformes (passerines) includes over 5000 species of bird, making up approximately 60% of all bird species [7-9]. Among them, the zebra finch (*Taeniopygia guttata*), a frequently utilised model species, is also known to primarily use its hindlimbs to take to the air: previous studies showed that the hindlimb is responsible for producing 94% of their take-off velocity [2]. To date however, the detailed internal hindlimb mechanics necessary to produce a successful take-off remain largely unknown. This lack of knowledge in extant birds not only limits our understanding about how they master the feat of taking to the air but also presents an obstacle to accurately infer the capacity of fossil birds to be airborne, thus blurring our understanding of the origin of flight more generally.

Computational biomechanical modelling is a useful tool for calculating the internal mechanics occurring within a biomechanical system which are otherwise very difficult if not impossible to directly measure [10-15]. Moreover, the application of such computational analysis methods to extant animals is seen as a key strategy to systematically develop the sound biomechanical basis on which to further our understanding also of the conditions in extinct species [16-18]. The inverse analysis approach is one such computational method that takes measured kinematics and kinetics to drive a biomechanical model to calculate the internal moments at each degree of freedom of each joint [14, 19-22]. Detailed, 3D models of the musculoskeletal anatomy allow relating these external moments to the moment generating capacity of the internal force generating structures, i.e. the muscles, and to develop a more detailed understanding of internal avian hindlimb kinetics during the take-off leap. However, few

3

62   studies have reported on the detailed external kinetics (ground reaction forces) [2, 4-6] associated

63   with the avian take-off leap and even fewer studies have investigated 3D hindlimb kinematics for these

64   activities [1]. The authors are aware of only a single study that has investigated the biomechanics of

65   the avian jump, focussing on a predictive simulation of the ground dwelling elegant-crested tinamou

66   *Eudromia elegans* [23]. However, due to the scarcity in ground reaction forces and kinematic data of

67   the tinamou leap, data on which an inverse analysis would rely on, the authors opted for a forward

68   approach to predict the leaping behaviour. In how far the simulations reflect kinetics and kinematics

69   that are consistent with actual conditions that can be observed and measured in this bird therefore

70   remains to be established. Although computational analyses in birds are available and have shown the

71   value of such analyses to further our understanding of avian hindlimb biomechanics with respect to

72   e.g. the critical role of the ankle muscles in the take-off leap of the tinamou and the function of the

73   antitrochanter as a passive mechanism to stabilise the hip of the running ostrich [23, 24], to date no

74   study has determined the internal hindlimb joint kinetics of a flying bird as it leaps into the air using

75   detailed measurements of external forces and hind limb kinematics. With the application of X-ray

76   reconstruction of moving morphology (XROMM) technology to capture detailed 3D bone kinematics

77   of the avian take-off leap, in combination with computational biomechanical analyses, the technology

78   is finally available to accurately simulate the internal mechanics of the extant avian take-off [1, 10, 16,

79   25-28].

80   The current study therefore combines external forces and detailed bone kinematics that feed into

81   computer simulations into the biomechanics of the hindlimb throughout the take-off leap of the zebra

82   finch. In doing so we aim to address the following hypotheses that help to develop a comprehensive

83   understanding of the mechanical requirements birds need to meet to propel themselves into the air.

84   We firstly hypothesised that in order to generate the motion of the avian take-off leap, characterised

85   by the hip, knee, and ankle joints all extending until the bird is airborne [1, 3], net external flexion

86   moments of similar peak magnitudes act at all these joints which the muscles balance by exerting

87   extension moments. Consistent with the observation that predicative simulations of the tinamou

88   predict the ankle to be most critical in determining the success of the take-off leap in a ground-

89   dwelling bird [23], we further hypothesised that the ankle extensors of the zebra finch possess the

90   largest capacity to balance the external moments. Finally, considering the avian hips' powerful

91   capacity to generate internal/external rotation (IER) moments and a poor capacity to generate

92   abduction/adduction (ABAD) moments [10, 16, 24] in the presence of the antitrochanter, we

93   hypothesise that external moments of similar peak magnitudes act in IER/ABAD on the hip joint of the

94   zebra finch and that the bird possess powerful ability to actively balance the IER moments.

95

Materials and methods

97 To address our hypotheses, we built upon previously published detailed kinetics and kinematics data

98 of the take-off leap of the zebra finch as input to a biomechanical simulation of the avian take-off leap

99 [1, 2] as explained in more detail below.

Overview

101 Key steps of our analysis methodology included the use of CT scans of the same individual, together

102 with additional morphological data in the literature to characterise the bone and musculature

103 respectively, from which a detailed 3D musculoskeletal model of the zebra finch hindlimb was

104 developed. Here, muscles were mapped from a previously published magpie musculoskeletal model

105 on to the zebra finch skeleton [10, 29, 30]. In addition, previously published 3D kinematics and ground

106 reaction forces were used to drive the musculoskeletal model in inverse dynamics analyses to estimate

107 external joint moments [1, 2]. The combination of these unique datasets, collected from the same

108 species and even the same individual, offered a unique opportunity to generate an accurate simulation

109 of the zebra finch take-off biomechanics.

110 The external joint moments were compared against the moment generating capacity of the muscles

111 to document the biomechanical requirements and to assess the zebra finch's capability to actively

112 balance the hindlimb joint moments experienced throughout the take-off leap. Here, moments about

113 hip flex/extension (FE), ab/adduction (ABAD), int/external rotation (IER) and moments about FE at

114 both the knee and ankle joints were considered. In addition, by comparing the hindlimb morphology

115 and ground reaction forces of a variety of passerines ranging in mass (zebra finch *Taeniopygia guttata*,

116 15.4 g, starling *Sturnis vulgaris*, (77.3 g), crow *Corvus corone* (440 g) and raven *Corvus corax*, 1.1 kg) it

117 was possible to explore the take-off mechanics of passerines more generally.

Materials, model building, and musculoskeletal analysis approach

119 The computational biomechanical musculoskeletal model of a zebra finch (15.4 g) was developed

120 based on CT scans and muscle data of corvids from previously published works [1, 10, 29]. The CT data

6

121 was used for establishing the 3D skeletal model. In order to describe the spatial relationships between

122 bones, local coordinate systems were established based on shape fitting techniques and functional

123 analyses of the joints [31], as detailed in the supplementary information (S1A). Muscles were modelled

124 by 3D lines of action [12, 32, 33] by mapping muscles from the magpie skeleton to the zebra finch

125 using elastic registration [34], while muscle maximum isometric force was scaled by body mass.

126 Detailed kinematics derived from previously published XROMM data [1] were then used together with

127 ground reaction forces [2] of zebra finch take-off leaps to drive the model in inverse dynamics

128 simulations to calculate the external moments acting at the hindlimb joints. Nine sets of ground

129 reaction forces obtained from 9 jumps of 4 birds (15.4±1.8g), were temporally synchronised with two

130 sets of kinematics trials (taken from 1 bird with a mass of 15.4 g), resulting in 18 simulations analysed.

131 Muscle moment arms were measured and used to calculate the maximum moment generating

132 capacity about hip flexion/extension, ab/adduction and internal/external rotation, and knee and ankle

133 flexion/extension. The muscle moment generating capacity was compared to the external joint

134 moment to ascertain the zebra finch's ability to balance the external joint moments.

Skeletal model

136 The skeletal model was derived from CT scans (isotropic resolution 0.04mm) of a zebra finch

137 *Taeniopygia guttata* specimen (15.4 g), obtained in previously published studies (for full details please

138 refer to [1]). For the current study, bones were segmented using ITK-SNAP [35], and imported in to

139 Rhino (v7; Robert McNeel & Associates, Seattle, USA) [36] where triangulated bone surfaces were

140 obtained after fitting subdivision surfaces using the QuadRemesh function. Bones which were treated

141 in this way were the pelvis, femur, patella, tibiotarsus and tarsometatarsus. The detailed definition of

142 joint centres and axes and local bone coordinate systems are available in the supplementary

143 information (S3).

144 A linked rigid body model with 4 segments including the pelvis, thigh, shank and tarsometatarsus was

145 defined in OpenSim v4.1 [37]. Here, body segments were linked by 3 joints (hip, knee and ankle joints)

146   with 3 rotational degrees of freedom (DoF) at the hip (allowing flexion/extension, internal/external

147   rotation and ab/adduction) and 2 DoF at each of the knee and ankle joints (allowing flexion/extension

148   and internal/external rotation). Because the foot remained stationary on the perch and motion of the

149   trunk was largely due to the extension of the hip, knee and ankle joints, the foot was not included as

150   a dedicated structure of the musculoskeletal model. In order to better capture the mechanics of

151   hindlimb extension, a biomechanical model of the patella-femoral joint was incorporated in to the

152   model. Here, the motion of the patella was defined by a 3D spline curve following approximately the

153   trochlear surface of the femur. The patella was allowed to move along that spline as a function of the

154   knee angle, with details of the motion informed by a musculoskeletal model of the helmeted

155   guineafowl *Numida meleagris* [38]. In order to map patellar motion from the guineafowl to the zebra

156   finch model, the femoral surface of the guineafowl model was elastically registered to the zebra finch

157   femur [39]. The parameters of the elastic registration were then used to map the spline defining

158   patellofemoral motion from the guineafowl to the zebra finch model using the R-package MesheR

159   [34].

Muscle geometry

161   The musculoskeletal model of the zebra finch included 43 muscles crossing the hip, knee and ankle,

162   which were modelled as 3D polylines spanning origin and insertion using via points to fully describe

163   their curved paths (Figure 1). Magpies (*Pica pica*) and zebra finch, share broadly similar hindlimb

164   myology both following the characteristic hindlimb morphology of passerine birds [9]. Muscle

165   attachment sites and via points were therefore mapped from a previously established model of the

166   magpie [10] to the zebra finch hindlimb. Using a non-rigid iterative closest point (ICP) registration [39]

167   the magpie femur, tibiotarsus and tarsometatarsus were elastically registered to the corresponding

168   long bones of the zebra finch hindlimb [34] (Figure 2). Using 3D Slicer 4.11 [40], the pelvis of the

169   magpie and zebra finch were first split in to the ilium, ischium and pubis before elastically registering

170   them onto each other following the same approach as described for the long bones above. Following

171   non-rigid registration, the rigid transformation and isotropic scaling parameters were recovered using

172 Ordinary Procrustes Analysis (OPA) [41] computed between the vertices of the original magpie bone

173 surface and the vertices of the magpie bone surface that was elastically registered to the respective

174 zebra finch bone (Matlab (2019b, The Mathworks, Nantucket, USA). This step was encoded in a 4x4

175 homogeneous transformation matrix. The remaining difference between the positions of the OPA

176 mapped vertices and their elastically registered counterparts was captured in a dense deformation

177 field. The homogeneous transformation matrix and the dense deformation field were then applied to

178 all attachment and via points of the magpie muscles associated to the respective bone surface using

179 the R-package MesheR [34], and in so doing mapping muscles from the magpie hindlimb to the zebra

180 finch (Figure 2). Wrapping cylinders and spheres were added with positions, orientations and radii

181 individually adjusted to define the 3D muscle paths throughout the jumping RoM that avoided any

182 intersection of muscles with bones.

183 Biomechanical analysis

184 Kinematics

185 Detailed 3D kinematics were derived from previously published X-ray reconstruction of moving

186 morphology (XROMM) data of the left hindlimb throughout two autonomous take-off leaps of the

187 zebra finch [1]. For these analyses three tantalum bead markers with an approximate diameter of 0.5

188 mm were attached to the tarsometatarsus, while two markers were implanted to the tibia, one to the

189 femur, and one at the pelvis. In order to reliably track 3D skeletal kinematics for the current study, the

190 location of the pelvis was determined using the implanted pelvic marker and, while its orientation was

191 determined using scientific rotoscoping, a reliable process in particular for bones with specific shapes

192 such as the pelvis [42]. Owing to the generally higher precision of the 3D marker positions compared

193 to 3D position and orientation data derived from scientific rotoscoping [1, 42], a method for

194 reconstructing 3D skeletal motion that maximised usage of the marker data while minimising reliance

195 on the manual process of scientific rotoscoping was developed. Here, 3D positions and orientations

196 of the long bones of the hindlimb were obtained using the attached physical markers, supplemented

197   by functionally defined virtual markers, and detailed 3D bone surface models. A full detailed

198   description of the methodology used to define these virtual markers and track 3D skeletal motion

199   using a combination of XROMM data, bone surfaces and virtual markers is provided in the

200   supplementary materials section (S1, S2).

201   An inverse kinematics analysis was then carried out in OpenSim [22, 32, 37] to map the kinematics

202   from the XROMM data to the constrained biomechanical model using physical and virtual markers

203   placed at their known locations on the model bones. Across the two kinematics trials, the ranges of

204   motion for the skeletal kinematics with respect to hip flexion/extension (FE), abduction/adduction

205   (ABAD) and internal/external rotation (IER) recovered in that manner were 42° (-4° to 38°), 15° (-37°

206   to -22°), and 20° (8° to 28°), respectively. Knee and ankle FE range of motion were 40° (123° to 163°)

207   and 74° (61° to 135°), respectively (see supplementary figure SF1). Substantial internal/external

208   rotation range of motion at the knee and ankle was also measured, with a range of motion of 16° (5°

209   to 21°) and 30° (-15° to 15°), respectively.

210   The take-off velocity of the bird was defined by measuring the velocity of its centre of mass at the

211   instant the feet left the ground [2, 3, 6]. To that end, the centre of mass of the zebra finch was

212   determined using the soft tissue envelope of the zebra finch and the RigidBodyParams [43] function

213   under the assumption of a homogenous body soft tissue density [43]. The velocity of the centre of

214   mass of the zebra finch was then measured by tracking its location throughout the take-off trials using

215   the OpenSim 4.1 BodyKinematics Tool. Take-off velocity was determined as the velocity at the instant

216   all toes on the hindlimb being tracked, left the perch. Take-off velocities for the two trials investigated

217   were determined to be 1.39 and 1.08 m/s.

218   Kinetics

219   Previously reported ground reaction forces of the take-off leap of a zebra finch [1] were used as inputs

220   to the current study in this study. Since full details for the collection of these data were previously

221   reported, the experimental setup is only briefly summarized below. Vertical and horizontal ground

222   reaction forces were recorded at 400 Hz from a force platform (Squirrel force plate, Kistler France, Les

223   Ulis, France; resolution ±0.01N), to which a wooden perch, 1.5 cm in diameter, was attached. The

224   ground reaction forces measured from nine trials of a zebra finch taking off from a perch [2] were

225   used to drive the take-off simulations.

226   Each of the nine zebra finch kinetics trials were paired with the two sets of kinematics trials enabling

227   analysis of 18 distinct take-off conditions. Here, the ground reaction forces were temporally aligned

228   to the kinematic data such that at the instant at which the resultant ground force fell to zero was

229   matched to the instant at which the toes left the ground. Ground reaction forces were assumed to act

230   through the centre of the perch (Figure 3).

231   For use in the current study, the ground reaction force vectors were scaled in magnitude so that the

232   impulse imparted by the leg resulted in 94% take-off velocity that was measured from the kinematics

233   for the two trials considered here. This scaling was performed to reflect previously identified

234   relationships for the take-off mechanics of the zebra finch [2]. Here, the method for calculating the

235   velocity as a result of the impulse (V_{GRF}) imparted by the hindlimb followed the approach by Provini

236   and colleagues (2012) and is outlined below. Firstly, the acceleration resulting from the ground

237   reaction forces, $\dot{V}_{GRF}$, were calculated as follows:

238
$$\dot{V}_{GRF} = \frac{\sqrt{F_x^2 + F_y^2 + (F_z^2 - mg)}}{m} \qquad (2)$$

239   where F_x is forward force, F_y is lateral force, F_z is vertical force, m is the mass of the bird, and g is the

240   acceleration due to gravity. The integral of the acceleration over the duration of the take-off then

241   provides the take-off velocity as a result of the ground reaction forces, V_{GRF}:

242
$$V_{GRF} = \int_{t_0}^{lo} \frac{\sqrt{F_x^2 + F_y^2 + (F_z^2 - mg)}}{m} dt \qquad (3)$$

243   where t_0 is the time when the jump starts and lo the time at lift off.

244   External joint moments

245   Ground reaction forces were applied to the tarsometatarsus, with the centre of pressure placed in the

246   centre of the perch (Figure 3). Using kinematics and ground reaction forces as input to the inverse

247   dynamics analysis, external joint moments were calculated about hip FE, ABAD, IER, knee FE and ankle

248   FE. Joint moments were normalised by the product of bodyweight and leg length L (defined as the

249   sum of the segment lengths of femur, tibiotarsus, tarsometatarsus, and digit III) [44], and time

250   normalised to the duration of the jump cycle. Mean and standard deviations of the external joint

251   moments were calculated across all 18 take-off sequences to obtain a robust estimate of the envelope

252   of zebra finch take-off biomechanics. Here, joint moments are identified by the direction of joint

253   movement induced by the action of the muscle group activating the respective degree of freedom.

254   Muscle moment generating capacity

255   The methodology for calculating muscle moment generating capacity followed the approach

256   described by Meilak and colleagues (2021) and is outlined below. The moment generating capacity for

257   each muscle about each joint degree of freedom (DoF) being considered was calculated by multiplying

258   the muscle maximum isometric force (F_{max}) by the instantaneous moment arm ($MA_{t,i,j}$), evaluated

259   at each time increment (*t*) throughout the kinematics trials. These moments were evaluated for each

260   muscle *i (where i=1..43)* as the product of the maximum isometric muscle force (F_{max}) and the

261   instantaneous moment arm ($MA_{t,i,j}$) determined throughout the take-off kinematics for each

262   rotational DoF *j (where j=1..5* for hip FE, ABAD, IER, knee FE and ankle FE):

263    $$M_{t,i,j} = F_{max,i} \cdot MA_{t,i,j} \qquad (4)$$

264   The moments of muscles acting in the same direction (i.e. their moments have the same sign) were

265   summed for each degree of freedom to provide the total joint moment generating capacity in relation

266   to that specific action ($M_{t,j}$):

267    $$M_{t,j} = \sum_{i=1}^{43} M_{t,i,j} \qquad (5)$$

12

268   Comparing biomechanical conditions across the group of Passerine birds

269   To allow comparative analysis of conditions across the Passerine clade, the ground reaction force data

270   available for the zebra finch was amended with similar data from further animals within the group of

271   passerines. In a study approved by the local ethics committee of the University of Southampton (ERGO

272   II ID 32207), a crow (*Corvus corone*) and raven (*Corvus corax*) took off 6 times each from a force

273   platform (9260AA, Kistler) while 3D ground reaction forces (GRFs) were sampled at 10 kHz. For all

274   species, vertical and horizontal forces were filtered using a zero-phase low-pass (40Hz) custom filter

275   in Matlab. The peak ground reaction forces of the zebra finch, starling [3], crow and raven were all

276   normalised by bodyweight and, together with key measures of hind limb geometry (Table 2) to

277   compare take-off conditions within the group of passerines.

278

Results

280 The duration of the take-off leap ranged between 62-65ms (Figure 4). Mean resultant peak ground

281 reaction forces per leg were 1.81±0.21 BW (range: 1.42 to 2.15 BW, c.f. supplementary figure SF1) and

282 occurred at about 62 % leap cycle time. Across the two kinematics trials, the largest ranges of motions

283 were 74°, 42° and 40° about the ankle, hip, and knee FE axes, respectively. The ranges of motion about

284 the joints' secondary degrees of freedom were similar, with hip IER and ABAD RoMs of 20° and 15°,

285 respectively and knee and ankle IER RoMs of 16° and 30°, respectively (see supplementary figure SF2).

286 The largest external moments observed were the moments around the flexion/extension axes. Here,

287 the mean peak external joint flexion moments at the hip and ankle were of similar magnitude

288 (0.66±0.04 and 0.68±0.05 BWL, respectively) while the mean knee extension moment was only about

289 half that value (0.38±0.05 BWL, Figure 5, Table 3). The smallest peak moments were computed about

290 hip IER and ABAD with mean peak moments of 0.27±0.07 and 0.20±0.07 BWL, respectively (Figure 5,

291 Table 3). At the instances that these peak moments occurred, the muscles had the ability to generate

292 120%, 282% and 61% of the mean peak hip FE, IER and ABAD joint moments, respectively (Figure 5

293 Table 3). The muscles were able to generate 177% and 176% of the mean peak joint moments about

294 the FE axes of the ankle and knee, respectively (Figure 5 B and C, Table 3).

295 Comparing conditions across the group of passerines, the zebra finch as bird with the smallest mass

296 by far (15.4 g) had the smallest normalised peak ground reaction forces per leg of 1.94±0.25 BW, while

297 starling (77.3 g), crow (440 g), and raven (1.1 kg) exerted very similar peak GRFs with values of

298 2.15±0.14 BW [3], 2.20±0.29 BW, and 2.25±0.14 BW, respectively (see supplementary figure SF3).

Discussion

299   This is the first detailed investigation into the hindlimb mechanics of a flying bird as it takes to the air

300   with a take-off leap using modern biomechanical analyses. The model presented here simulated 18

301   distinct take-off trials of a zebra finch's take-off leap from a perch covering a range of take-off

302   conditions in a passerine bird, the group that makes up approximately 60% of all extant bird species

303   [7-9]. In doing so our study revealed a consistent pattern of internal mechanics across the trials that

304   was characterised by the largest peak external moments occurring around the FE axis of the hip and

305   ankle (requirements, 0.68 and 0.66 BWL, respectively), while considerably smaller external moments

306   were observed about the FE axis of the knee, amounting to only 56% of the respective peak moments

307   at the hip. On the other hand, peak hip IER and ABAD moments were 40% and 29% of peak hip FE

308   moments respectively. Together with previous findings regarding the substantial extent of joint range

309   of motion in IER exercised by birds [1, 27] and the substantial moment generating capacity of the hip

310   joint muscles around that axis [10], these novel data on the internal hind limb mechanics during the

311   take-off leap strongly support the notion that the execution and control of hindlimb motion in birds is

312   not limited to a single (sagittal) plane but is essentially 3D in nature [16].

313   Across the hip, knee and ankle FE degrees of freedom, the muscles had the ability to generate 120%,

314   176%, and 177% of the mean peak external joint moments, respectively. In relative terms therefore,

315   muscles spanning the hip were closest to reaching the capacity limit whilst muscles spanning the knee

316   and ankle joints had the largest reserves. Although for the most typical (mean) of the conditions

317   studied here the capacity of the muscles to generate moments was always larger than the

318   requirement (Figure 5), the closing gap between the upper limit of the 2.5 SD range of the external

319   hip flexion moments and available hip muscle extension capability suggests that more powerful take-

320   off leaps than those observed here would likely require further activation of the more distal, knee and

321   ankle joint spanning muscles for which the requirements remained more comfortably within their

322   capability [23]. An explanation as to why capacity to balance the moments at the more distal joints

324   retains a larger reserve may be found in the design of the avian hindlimb and specifically the biarticular

325   muscles [45-47]. Such biarticular muscles include in particular the m. caudofemoralis pars caudalis

326   (MFCLP), m. flexor cruris medialis (MFCM) and m. iliofibularis (MIF) which span the caudal side of the

327   hip and knee (Figure 1, Table 1). MFCLP and MFCM form a major part of the hip extensor moment

328   generating capacity, together generating 35% of the total hip extensor moments whereas the MIF has

329   a greater role as a hip abductor, generating 20% of the muscle abduction generating capacity [10].

330   Whilst during the take take-off leap of the zebra finch the hip, knee and ankle are all extending (Figure

331   SF1), the muscles need to generate a net knee flexion moment, suggesting that knee flexors may be

332   activated. Biarticular muscles, which if activated generate an extension moment at the hip but a

333   flexion moment at the knee such as the MFCLP and MFCM, would thus appear to be prime candidates

334   for meeting the demands during the take-off leap. Moreover, co-activation of knee flexors and

335   extensor muscles (muscle co-contraction) though energetically less optimal, may help to increase

336   compressive forces across the knee joint and help to lock or at least minimise the extent of

337   internal/external rotation [27, 28, 48]. Further analysis to examine muscle activation patterns, though

338   beyond the scope of the current work, could corroborate whether activation of these biarticular

339   muscles to extend the hip and generate the extension moment applied to the knee suggested by the

340   analyses here does indeed occur and help to further elucidate how avian hindlimb muscles are

341   orchestrated during the take-off leap.

342   Here, it is also informative to consider absolute moments where indeed the ankle extensors had the

343   largest joint moment generating capacity, capable of generating peak total extension moments of up

344   to 1.18 BWL at the ankle, followed by the hip extensors, with a peak total capacity of 0.81 BWL. The

345   passerine bird ankle muscles' capacity to produce the largest moments indicates the importance of

346   the ankle joint throughout the take-off, a finding in line with previous research on the ground dwelling

347   elegant-crested tinamou *Eudromia elegans* [23] where the take-off heavily depended on the

348   parameters and activation of the ankle extensors. Though to the authors knowledge no similar studies

349   reporting internal mechanics during a take-off leap of a flying bird are available for comparison, similar

16

350   analyses have been performed in ground-dwelling birds such as the emu and the ostrich. Here, data

351   on the running of the ostrich obtained using similar analysis methods revealed that the peak

352   normalised FE moments across all of the hip, knee, and ankle joint of the ostrich were considerably

353   smaller than those reported during the take-off leap of the zebra finch reported here. The largest

354   differences in normalised moment magnitudes were observed for the ankle and hip joints where the

355   peak moments during running in the ostrich amounted to only 24% (0.16 BWL) and 25% (0.17 BWL)

356   of the values for the zebra finch leap. The external moment at the knee during running in the ostrich

357   was the largest of all 3 hindlimb joints with 0.20 BWL yet amounted to only about 53% of the value

358   the current study calculated for the take-off leap of the zebra finch. In the comparison of the absolute

359   moment magnitudes it is important to consider that speed at which the ostriches were running was

360   rather slow (3.24 m/s) compared to the maximum speed ostriches can achieve (about 13.9 m/s) and

361   higher speeds will be associated with higher external forces and moments. However, not only absolute

362   magnitudes but also the ratios of their magnitudes at the hip, knee, and ankle differed between the

363   zebra finch take-off leap and ostrich running. While the largest external moment during running of the

364   ostrich was computed at the knee, suggesting that that ostrich running is knee driven, the external

365   knee moment during the take-off leap of the zebra finch was the smallest of all the hind limb joints.

366   For the zebra finch leap, peak moments were observed at the hip and ankle suggesting that this

367   motion is hip and ankle driven instead and signifying that an interesting avenue for future work would

368   be to investigate whether the different motor behaviours are indeed associated with different muscle

369   coordination patterns and that care must be taken when speculating about design principles and

370   interpreting optimality of the musculoskeletal system based on a limited repertoire of motor

371   behaviours.

372   Previous studies have demonstrated that avian pelvic muscles have a considerable capacity to produce

373   IER moments at the hip [10, 16, 49]. The current study revealed not only that substantial external

374   moments about the IER axis occur during the take-off leap of the zebra finch, approaching 40% of the

375   hip extension moment, but also demonstrated that the hip muscles had the greatest relative capacity

376   to actively balance these moments, with muscles capable of generating up to 280% of the mean peak

377   external IER moments. Together these data provide further evidence that IER rotation is actively

378   controlled during routine, straight line take-off leap of passerine birds. The ample capacity of the

379   muscles to enable IER during such jumps further allows for take-off leaps to occur with substantially

380   more axial turning/rotation while the bird remains on the ground, offering the bird a wider repertoire

381   of take-off and escape behaviours. On the other hand, foraging behaviours have been shown to be

382   linked with substantial extents of hindlimb IER [27] and it may well be that substantial IER capability

383   of the hip muscles are particularly crucial in supporting those behaviours (particularly for single limb

384   support) in addition to allowing variation in the take-off leap.

385   In contrast to the well powered hip IER DoF during the take-off leap, the pelvic muscles of the zebra

386   finch were only able to balance 61% of the peak mean external adduction moments. Analysis of the

387   relationship of the relative moment generating capacity of the avian hip muscles do indeed

388   demonstrate that the smallest capacity to generate a moment exists with respect to the ABAD axis.

389   However, even though the avian hip has a relatively limited capacity to actively produce hip ABAD

390   moments, birds can rely on a passive mechanism using the antitrochanter and associated ligamentous

391   structures to balance external abduction moments [49]. The utilisation of the antitrochanter is also a

392   feature in the hip mechanics of the ostrich: though substantial external abduction moments are

393   generated during walking and running in these flightless birds, the design of the hip allows to stabilise

394   the joint passively such that ostriches neither require nor possess muscles to do so actively [49, 50].

395   The antitrochanter is indeed a feature shared across all extant birds that was not present in some of

396   the very earliest birds such as *Archaeopteryx*, who likely relied on powerful hip adductors to generate

397   the required adduction moments [16].

398   Maintaining substantial lever arms of the muscles throughout the functional range of motion of a joint

399   is a prerequisite to maintain high levels of muscle capacity to generate moments. Passive structures

400   can play a key role to help maintaining muscle lever arms include sesamoid bones such as the patella

401 which is key to enable joint function in flexion at the knees in human and avian bipeds [33, 46] The

402 hypotarsus is another anatomical feature of the avian hindlimb that helps to guide tendons around

403 the ankle joint and to and maintain their lever arms [51]. The posterior side of the ankle further

404 includes the cartilagio tibialis which constrains the muscle line of action to act further away from the

405 joint axis of rotation thus helping to maintain its moment [29]. The model presented here therefore

406 modelled the patellofemoral joint in an approach informed by the birds' bone surface anatomy and

407 kinematic model data from the literature [38] and in incorporated these passive structures of the ankle

408 with wrapping objects and via points informed by CT scans.

409 The relative peak ground reaction forces during the take-off leap of all passerines considered here

410 were rather similar in magnitude, despite the large range in body mass. During the take-off leap the

411 zebra finch (15.4 g), starling (77.3 g), crow (440 g) and raven (1.1 kg) generated peak ground reaction

412 forces per leg of 1.94±0.25 BW, 2.15±0.14 BW [3], 2.2±0.29 BW, and 2.25±0.14 BW, respectively.

413 Similarities do not stop with the ground reaction forces but are also apparent in the morphology of

414 their hindlimbs. The passerines considered here, the zebra finch, starling, crow, and raven, possess

415 very similar hindlimb indices, a measure of relative segment lengths of the hindlimb ((tarsometatarsus

416 length + tibiotarsus length) / femur length [52]) with values of 2.64, 2.84, 2.75, and 2.63, respectively

417 [53] (Table 2). The similarities in normalised leg segment lengths and ground reaction forces spanning

418 a range of passerines, which differ in mass by approximately two orders of magnitude, support the

419 hypothesis that passerines share a similar take-off behaviour, as reported here. Forward dynamics

420 simulations of the tinamou (0.55 kg) leaping predict similar but somewhat higher peak ground reaction

421 forces of 2.62 BW per leg during the jump [23]. On the other hand, predicted joint kinematics profiles

422 for the take-off leap of the tinamou demonstrated ranges of motion at the hip knee and ankle of 65°,

423 91° and 109° respectively, consistently greater than the range of motion measured in the zebra finch

424 (42°, 40° and 74° respectively), while the hindlimb index of the tinamou *Eudromia elegans* (belonging

425 to the group Tinamiformes) was 2.21, substantially smaller than that of the passerines considered

426 here. The relative difference in relative leg morphology between the passerines and tinamou could be

19

427   one of the determining factors resulting in the variability in take-off mechanics between the clades of

428   birds.

429   The kinematics used to drive the take-off simulation were informed by previously obtained XROMM

430   data of the zebra finch take-off leaps [1]. In this study, the use of the tantalum bead markers, detailed

431   bone surface geometry from high resolution μCT, and anatomical-functional relationships [31, 54]

432   were all used to increase repeatability in tracking 3D skeletal kinematics and reduce the influence of

433   the user during scientific rotoscoping [42]. Across the two kinematics trials, the difference between

434   the originally published orientation angles of the femur, tibiotarsus and tarsometatarsus was smallest

435   about FE and ABAD axes of the bones, with mean differences ranging from 0.6±0.5° to 3.3±2.7°. The

436   degree of freedom most difficult to determine during scientific rotoscoping was IER due to the

437   cylindrical shape of the long bones. Predictably, the largest difference was observed when comparing

438   the bone IER orientations, with mean differences in IER orientations across the three long bones

439   ranging from 7.3±4.8° to 11.5±6.3°. Differences in bone locations between the two methods were

440   minimal, mean differences across all three long bones ranged between 185 – 333 microns.

441   Due to the limited number of specimens in which sufficient bones had had a minimum of three

442   tantalum markers attached, only two sets of kinematics trials were used in this study. However, by

443   pairing each set of kinematic trials with nine sets of kinetics trials, we maximised the variability in take-

444   off conditions studied here. Future studies, using XROMM to capture detailed kinematics of passerines

445   should ensure that at least one of the long bones includes at least 3 markers to reduce the reliance on

446   the user during scientific rotoscoping. The simulations here included IER motion of the knee and ankle

447   joints, however the active muscle actuation of these degrees of freedom was not considered in line

448   with previous studies and under the assumption that typically small moments are balanced by passive

449   structures such as ligaments [37, 55]. Previous studies reported the take-off velocity of the zebra finch

450   to be around 1.7m/s [2, 6] which is faster than the take-off velocity, measured here from the XROMM

451   data which ranged between 1.08-1.39 m/s. Previously published studies measuring the kinematics of

452 animal subjects using implanted markers have reported the markers causing a limp [14]. The

453 comparatively slower take-off velocities reported here could thus be attributed to a response to the

454 implantation of the tantalum bead markers on the hindlimb bones. However, varying levels of

455 motivation between experimental conditions may also explain the observed difference and the similar

456 protocols using tantalum bead markers have been used to study a range of motor behaviours in birds

457 [46, 56, 57]. This study did not include the mechanics of phalanges in the analysis, as the take-off

458 trajectories of the hindlimb are defined primarily by the motion at the more proximal hindlimb joints

459 where also more substantial joint moments are generated. Future studies which may consider hind

460 limb mechanics during landing, when the detailed mechanics of foot are likely to play a more

461 important role, should aim to capture the detailed kinematics of the phalanges.

462 This study considered the maximal moment generating capacity of the muscles, taking into account

463 the muscle maximum isometric force and instantaneous moment arm throughout the take-off leap

464 and contrasted these to the external moments applied to the joints of the hind limb. In this way

465 general patterns of mechanical requirement and hindlimb muscles capability to meet the

466 requirements of a take-off leap were analysed. Although the sensitivity of muscle moment generating

467 capacity with respect to uncertainty in the definition of muscle geometry was not directly investigated

468 in this study, a thorough sensitivity analysis was performed for pelvic muscles in the magpie hindlimb

469 model that was the basis for the current study [10], which, given the similarity in overall hindlimb

470 design and specific hindlimb bone morphology, can reasonably be expected to remains valid for the

471 musculature of the zebra finch model here. Though the determination of the detailed muscle

472 activation patterns to balance the external moments was not within the scope of the current study,

473 further analyses of the biomechanical model (such as static optimisation [15, 32, 37]) would help to

474 further elucidate the detailed activation patterns of individual muscles as well as providing estimates

475 for the likely bon-on-one joint contact forces being transferred at le large joints of the avian hind limb

476 during a take-off leap.

477   This study is the first to establish the biomechanical requirements of the hindlimb of a flying bird as it

478   takes to the air. We present biomechanical conditions that hindlimbs of passerines, a clade of birds

479   that include over half of all avian species, experience during take-off. The zebra finch take-off leap is

480   primarily hip and ankle driven, which is in direct contrast to ostrich running mechanics which indicates

481   avian running is a primarily knee driven activity. The ability of the zebra finch muscles to produce over

482   double the mechanical requirements at the ankle and knee axes and about 20% more than the

483   requirements about the hip FE axis along with the suspected use of biarticular muscles and passive

484   structures is consistent with the hypothesis that the take-off leap as reported here is an optimized

485   way for the zebra finch to take to the air. Striking similarities in ground reaction forces and relative leg

486   morphology of multiple passerines suggest that the take-off behaviour described here could be shared

487   across all passerines, despite differences in mass by two orders of magnitude.

488   **Acknowledgements**

496

Tables

Table 1 Musculotendon units included in the musculoskeletal model of the zebra finch, grouped by which joints they cross; H, K and A denote the hip, knee and ankle joints, respectively. Muscles which are categorised under two joints are biarticular. Maximum isometric force was calculated by scaling the maximum isometric force of the corresponding muscles of the magpie by mass [10].

Abbreviation	Muscle name	Joints	Maximum isometric force [N]
MCFC	*M. caudofemoralis pars caudalis*	H	0.154
MFCLA	*M. flexor cruris lateralis pars accessoria*	H	0.250
MISF1	*M. ischiofemoralis 1*	H	0.259
MISF2	*M. ischiofemoralis 2*	H	0.259
MISF3	*M. ischiofemoralis 3*	H	0.259
MITC1	*M. iliotrochantericus caudalis 1*	H	0.396
MITC2	*M. iliotrochantericus caudalis 2*	H	0.396
MITC3	*M. iliotrochantericus caudalis 2*	H	0.396
MITCR	*M. iliotrochantericus cranialis*	H	0.003
MITM	*M. iliotrochantericus medius*	H	0.057
MOL	*M. obturatorius lateralis*	H	0.112
MOM	*M. obturatorius medialis*	H	0.431
MPIFL	*M. puboischiofemoralis pars lateralis*	H	0.388
MPIFM	*M. puboischiofemoralis pars medialis*	H	0.448
MFCLP	*M. flexor cruris lateralis pars pelvica*	H, K	0.346
MFCM	*M. flexor cruris medialis*	H, K	0.238
MIC	*M. iliotibialis cranialis*	H, K	0.218
MIF	*M. iliofibularis*	H, K	0.458
MILcaudal1	*M. iliotibialis lateralis caudalis 1*	H, K	0.254
MILcaudal2	*M. iliotibialis lateralis caudalis 2*	H, K	0.254
MILcaudal3	*M. iliotibialis lateralis caudalis 3*	H, K	0.254
MILcranial1	*M. iliotibialis lateralis cranialis 1*	H, K	0.036
MILcranial2	*M. iliotibialis lateralis cranialis 2*	H, K	0.036
MILcranial3	*M. iliotibialis lateralis cranialis 3*	H, K	0.036
MFTI	*M. femorotibialis intermedius*	K	0.614
MFTL	*M. musculus femorotibialis lateralis*	K	0.013
MFTM	*M. femorotibialis medialis*	K	0.490
MFHL	*M. flexor hallucis longus*	K, A	0.843
MFPD2	*M. flexor perforates digiti 2*	K, A	0.357
MFPD3	*M. flexor perforates digiti 3*	K, A	0.362
MFPD4	*M. flexor perforates digiti 4*	K, A	0.483
MFPPD2	*M. flexor perforans et perforates digiti 2*	K, A	0.236

23

MGI	*M. gastrocnemius pars intermedia*	K, A	0.621
MGL	*M. gastroc-nemius pars lateralis*	K, A	1.824
MTCF	*M. tibialis cranialis caput femorale*	K, A	0.385
MEDL	*M. extensor digitorum longus*	A	0.031
MFB	*M. fibularis brevis*	A	0.366
MFDL	*M. flexor digitorum longus*	A	1.003
MFL	*M. fibularis longus*	A	0.861
MFPPD3	*M. flexor perforans et perforates digiti 3*	A	0.894
MGM	*M. gastrocnemius pars medialis*	A	1.153
MP	*M. plantaris*	A	0.079
MTCT	*M. tibialis cranialis caput tibiale*	A	0.516

502

Table 2. Key morphometric parameters of zebra finch (Taeniopygia guttata), starling (Sturnis vulgaris), crow (Corvus corone), and raven (Corvus corax).

species	mass [g]	femur length (L_{fem}) [cm]	tibiotarsus length (L_{tib}) [cm]	tarsometatarsus length (L_{tars}) [cm]	digit III length [cm]	hindlimb length [cm]	hindlimb index ((L_{tars} + L_{tib})/ L_{fem})
zebra finch	15.4	1.40	2.24	1.46	1.10	6.2	2.64
starling [3]	77.3	2.53	4.37	2.82			2.84
crow	440	5.28	8.74	5.77			2.75
raven	1100	6.92	11.42	6.80			2.63

Table 3 External joint moments and total muscle moment generating capacities of the zebra finch at the instances at which the peak external joint moments occur. To actively power the take-off leap by muscle action, the combined(total) moment generating capacity of all muscles must at least reach if not exceed the level of the external joint moments . Positive moments act in extension, external rotation, and adduction, while negative moments act in flexion, internal rotation, and abduction.

joint DoF	joint moment [BWL] (requirement)	total muscle moment generating capacity [BWL] (capacity to meet requirement)
ankle extension	0.66±0.04	1.18
knee extension	-0.38±0.05	-0.67
hip extension	0.68±0.05	0.81
hip internal rotation	-0.27±0.07	-0.75
hip abduction	-0.20±0.07	-0.12

Figure captions

Figure 1 The musculoskeletal model of the left zebra finch hindlimb included 43 musculotendon units. A) Muscles that either cross the hip or knee joint and biarticular muscles crossing both hip and knee joints are shown in a caudo-lateral view. B) Anterior and C) posterior view of muscles crossing the ankle joint and biarticular muscles crossing both knee and ankle joints. For an explanation of the abbreviations of the muscles used here, please refer to Table 1.

Figure 2 Schematic demonstrating the process of morphing the musculature from the magpie to the zebra finch hindlimb. To allow for a better visual comparison of the bones which differ by almost a factor of two in size, the bone surfaces depicted here are isotopically scaled by the reciprocal of the square root of their respective surface area. **A** Establishing an elastic mapping by comparing magpie and zebra finch bone surfaces. Here, magpie bones were first registered to the corresponding zebra finch bone using non-rigid iterative closest point (ICP) registration [39]. Following non-rigid registration, the rigid transformation and isotropic scaling parameters were recovered using Ordinary Procrustes Analysis (OPA) computed between the vertices of the original magpie bone surface and the vertices of the magpie bone surface that was elastically registered to the respective zebra finch bone. This step was encoded in a 4x4 homogeneous transformation matrix. The remaining difference between the positions of the OPA mapped vertices and their elastically registered counterparts was captured in a dense deformation field. **B** Application of the elastic mapping to muscle attachment and via point data. The homogeneous transformation matrix and the dense deformation field were then applied to all attachment and via points of the magpie muscles associated to the respective bone surface, resulting in an elastic registration of these structures to the zebra finch model.

Figure 3 Force and moment diagram for the zebra finch hindlimb, including the pelvis, femur, tibiotarsus and tarsometatarsus in a lateral view. The musculoskeletal model described the hip, knee and ankle as three, two and two degree of freedom joints respectively. The straight black arrow on the perch represents the ground reaction force acting through the centre of the perch. Curved arrows reflect external moments acting at the joints and are colour coded such that the orange arrows identify the moment about the joint's flexion/extension axes, blue arrows identify moments about a joints' internal/external rotation axis, and green arrow identifies the moments about the joints' ab/adduction axis. At the hip, the ground reaction forces consistently result in flexion, abduction and an internal rotation moments throughout the leap cycles. At the knee and ankle joints, the ground reaction forces result in extension, and flexion moments, respectively.

Figure 4 Lateral view of right zebra finch hindlimb throughout the normalised take-off leap cycle. The duration of the take-off jump duration ranged from 62 to 67 ms while all of the ankle, knee, and hip joint undergo substantial extension.

Figure 5 External joint moments at the hip, knee and ankle together with the total moment generating capacity of the muscles, plotted over normalised leap cycle time. Solid lines depict the mean external joint moments (requirements), bands depict ±2.5 standard deviations, while dashed lines depict the total moment generating capacity of the muscles (capacity). Colours are used to differentiate the axis around which the moments act, with orange representing flexion/extension, green ab/adduction, and blue internal/external rotation. Positive moments represent (internal/external) moments that act to extend, adduct, and internally rotate, respectively.

References

[1] Provini, P. & Abourachid, A. 2018 Whole-body 3D kinematics of bird take-off: key role of the legs to propel the trunk. *The Science of Nature* **105**, 12. (doi:10.1007/s00114-017-1535-8).

[2] Provini, P., Tobalske, B.W., Crandell, K.E. & Abourachid, A. 2012 Transition from leg to wing forces during take-off in birds. *J Exp Biol* **215**, 4115-4124. (doi:10.1242/jeb.074484).

[3] Earls, K.D. 2000 Kinematics and mechanics of ground take-off in the starling Sturnis vulgaris and the quail Coturnix coturnix. *Journal of Experimental Biology* **203**, 725-739.

[4] Bonser, R. & Rayner, J. 1996 Measuring leg thrust forces in the common starling. *The Journal of Experimental Biology* **199**, 435-439.

[5] Heppner, F.H. & Anderson, J.G.T. 1985 Leg Thrust Important in Flight Take-Off in the Pigeon. *Journal of Experimental Biology* **114**, 285-288.

[6] Tobalske, B.W. 2004 Take-off mechanics in hummingbirds (Trochilidae). *Journal of Experimental Biology* **207**, 1345-1352. (doi:10.1242/jeb.00889).

[7] Selvatti, A.P., Gonzaga, L.P. & Russo, C.A.d.M. 2015 A Paleogene origin for crown passerines and the diversification of the Oscines in the New World. *Molecular Phylogenetics and Evolution* **88**, 1-15. (doi:https://doi.org/10.1016/j.ympev.2015.03.018).

[8] Ricklefs, R.E. 2012 Species richness and morphological diversity of passerine birds. *Proceedings of the National Academy of Sciences* **109**, 14482. (doi:10.1073/pnas.1212079109).

[9] Raikow, R.J. 1987 Hindlimb Myology and Evolution of the Old World Suboscine Passerine Birds (Acanthisittidae, Pittidae, Philepittidae, Eurylaimidae). *Ornithological Monographs*, iii-81. (doi:10.2307/40166726).

[10] Meilak, E.A., Gostling, N.J., Palmer, C. & Heller, M.O. 2021 On the 3D Nature of the Magpie (Aves: Pica pica) Functional Hindlimb Anatomy During the Take-Off Jump. *Frontiers in Bioengineering and Biotechnology* **9**. (doi:10.3389/fbioe.2021.676894).

[11] Bergmann, G., Deuretzbacher, G., Heller, M., Graichen, F., Rohlmann, A., Strauss, J. & Duda, G.N. 2001 Hip contact forces and gait patterns from routine activities. *Journal of Biomechanics* **34**, 859-871. (doi:http://dx.doi.org/10.1016/S0021-9290(01)00040-9).

[12] Heller, M.O., Bergmann, G., Deuretzbacher, G., Dürselen, L., Pohl, M., Claes, L., Haas, N.P. & Duda, G.N. 2001 Musculo-skeletal loading conditions at the hip during walking and stair climbing. *Journal of Biomechanics* **34**, 883-893. (doi:10.1016/S0021-9290(01)00039-2).

[13] Heller, M.O., Taylor, W.R., Perka, C. & Duda, G.N. 2003 The influence of alignment on the musculo-skeletal loading conditions at the knee. *Langenbeck's Archives of Surgery* **388**, 291-297. (doi:10.1007/s00423-003-0406-2).

[14] Taylor, W.R., Ehrig, R.M., Heller, M.O., Schell, H., Seebeck, P. & Duda, G.N. 2006 Tibio-femoral joint contact forces in sheep. *Journal of Biomechanics* **39**, 791-798. (doi:10.1016/j.jbiomech.2005.02.006).

[15] Delp, S.L., Anderson, F.C., Arnold, A.S., Loan, P., Habib, A., John, C.T., Guendelman, E. & Thelen, D.G. 2007 OpenSim: open-source software to create and analyze dynamic simulations of movement. *IEEE transactions on bio-medical engineering* **54**, 1940-1950. (doi:10.1109/tbme.2007.901024).

[16] Allen, V.R., Kilbourne, B.M. & Hutchinson, J.R. 2021 The evolution of pelvic limb muscle moment arms in bird-line archosaurs. *Science Advances* **7**, eabe2778. (doi:10.1126/sciadv.abe2778).

[17] Hutchinson, J.R., Anderson, F.C., Blemker, S.S. & Delp, S.L. 2005 Analysis of hindlimb muscle moment arms in Tyrannosaurus rex using a three-dimensional musculoskeletal computer model: implications for stance, gait, and speed. *Paleobiology* **31**, 676-701.

[18] Bishop, P.J., Hocknull, S.A., Clemente, C.J., Hutchinson, J.R., Farke, A.A., Barrett, R.S. & Lloyd, D.G. 2018 Cancellous bone and theropod dinosaur locomotion. Part III—Inferring posture and locomotor biomechanics in extinct theropods, and its evolution on the line to birds. *PeerJ* **6**, e5777. (doi:10.7717/peerj.5777).

602   [19] Duda, G.N., Eckert-Hübner, K., Sokiranski, R., Kreutner, A., Miller, R. & Claes, L. 1997 Analysis of
603   inter-fragmentary movement as a function of musculoskeletal loading conditions in sheep. *Journal of*
604   *Biomechanics* **31**, 201-210. (doi:https://doi.org/10.1016/S0021-9290(97)00127-9).
605   [20] Goetz, J.E., Derrick, T.R., Pedersen, D.R., Robinson, D.A., Conzemius, M.G., Baer, T.E. & Brown,
606   T.D. 2008 Hip joint contact force in the emu (Dromaius novaehollandiae) during normal level
607   walking. *J Biomech* **41**, 770-778. (doi:10.1016/j.jbiomech.2007.11.022).
608   [21] Lund, K. & Hicks, J. 2012 Getting Started with Inverse Dynamics. In *OpenSim Documentation* (
609   [22] Pizzolato, C., Reggiani, M., Modenese, L. & Lloyd, D.G. 2017 Real-time inverse kinematics and
610   inverse dynamics for lower limb applications using OpenSim. *Computer methods in biomechanics*
611   *and biomedical engineering* **20**, 436-445. (doi:10.1080/10255842.2016.1240789).
612   [23] Bishop, P.J., Falisse, A., De Groote, F. & Hutchinson, J.R. 2021 Predictive simulations of
613   musculoskeletal function and jumping performance in a generalized bird. *Integrative Organismal*
614   *Biology*. (doi:10.1093/iob/obab006).
615   [24] Rankin, J.W., Rubenson, J. & Hutchinson, J.R. 2016 Inferring muscle functional roles of the
616   ostrich pelvic limb during walking and running using computer optimization. *Journal of The Royal*
617   *Society Interface* **13**. (doi:10.1098/rsif.2016.0035).
618   [25] Rubenson, J., Lloyd, D.G., Besier, T.F., Heliams, D.B. & Fournier, P.A. 2007 Running in ostriches
619   (Struthio camelus): three-dimensional joint axes alignment and joint kinematics. *Journal of*
620   *Experimental Biology* **210**, 2548-2562. (doi:10.1242/jeb.02792).
621   [26] Rubenson, J., Lloyd, D.G., Heliams, D.B., Besier, T.F. & Fournier, P.A. 2010 Adaptations for
622   economical bipedal running: the effect of limb structure on three-dimensional joint mechanics.
623   *Journal of The Royal Society Interface*. (doi:10.1098/rsif.2010.0466).
624   [27] Kambic, R.E., Roberts, T.J. & Gatesy, S.M. 2014 Long-axis rotation: a missing degree of freedom
625   in avian bipedal locomotion. *J Exp Biol* **217**, 2770-2782. (doi:10.1242/jeb.101428).
626   [28] Kambic, R.E., Roberts, T.J. & Gatesy, S.M. 2017 3-D range of motion envelopes reveal interacting
627   degrees of freedom in avian hind limb joints. *Journal of Anatomy* **231**, 906-920.
628   (doi:doi:10.1111/joa.12680).
629   [29] Verstappen, M., Aerts, P. & De Vree, F. 1998 Functional morphology of the hindlimb
630   musculature of the black-billed magpie, Pica pica (Aves, Corvidae). *Zoomorphology* **118**, 207-223.
631   (doi:10.1007/s004350050070).
632   [30] Hudson, G.E. 1937 Studies on the Muscles of the Pelvic Appendage in Birds. *The American*
633   *Midland Naturalist* **18**, 1-108. (doi:10.2307/2420619).
634   [31] Ehrig, R.M. & Heller, M.O. 2019 On intrinsic equivalences of the finite helical axis, the
635   instantaneous helical axis, and the SARA approach. A mathematical perspective. *Journal of*
636   *Biomechanics* **84**, 4-10. (doi:https://doi.org/10.1016/j.jbiomech.2018.12.034).
637   [32] Seth, A., Sherman, M., Reinbolt, J.A. & Delp, S.L. 2011 OpenSim: a musculoskeletal modeling and
638   simulation framework for in silico investigations and exchange. *Procedia IUTAM* **2**, 212-232.
639   (doi:https://doi.org/10.1016/j.piutam.2011.04.021).
640   [33] Trepczynski, A., Kutzner, I., Kornaropoulos, E., Taylor, W.R., Duda, G.N., Bergmann, G. & Heller,
641   M.O. 2012 Patellofemoral joint contact forces during activities with high knee flexion. *Journal of*
642   *Orthopaedic Research* **30**, 408-415. (doi:10.1002/jor.21540).
643   [34] Schlager, S. 2015 *mesheR: Meshing operations on triangular meshes*.
644   [35] Yushkevich, P.A., Piven, J., Hazlett, H.C., Smith, R.G., Ho, S., Gee, J.C. & Gerig, G. 2006 User-
645   guided 3D active contour segmentation of anatomical structures: Significantly improved efficiency
646   and reliability. *NeuroImage* **31**, 1116-1128. (doi:https://doi.org/10.1016/j.neuroimage.2006.01.015).
647   [36] McNeel, R. 2020 Rhinoceros 3D, Version 4.0. *Robert McNeel & Associates, Seattle, WA*.
648   [37] Seth, A., Hicks, J.L., Uchida, T.K., Habib, A., Dembia, C.L., Dunne, J.J., Ong, C.F., DeMers, M.S.,
649   Rajagopal, A., Millard, M., et al. 2018 OpenSim: Simulating musculoskeletal dynamics and
650   neuromuscular control to study human and animal movement. *PLOS Computational Biology* **14**,
651   e1006223. (doi:10.1371/journal.pcbi.1006223).

652 [38] Cox, S.M., Easton, K.L., Lear, M.C., Marsh, R.L., Delp, S.L. & Rubenson, J. 2019 The Interaction of
653 Compliance and Activation on the Force-Length Operating Range and Force Generating Capacity of
654 Skeletal Muscle: A Computational Study using a Guinea Fowl Musculoskeletal Model. *Integrative*
655 *Organismal Biology* **1**. (doi:10.1093/iob/obz022).

656 [39] Manu. 2021 nonrigidICP. *MATLAB Central File Exchange*.

657 [40] Fedorov, A., Beichel, R., Kalpathy-Cramer, J., Finet, J., Fillion-Robin, J.-C., Pujol, S., Bauer, C.,
658 Jennings, D., Fennessy, F., Sonka, M., et al. 2012 3D Slicer as an image computing platform for the
659 Quantitative Imaging Network. *Magn Reson Imaging* **30**, 1323-1341.
660 (doi:10.1016/j.mri.2012.05.001).

661 [41] Veldpaus, F.E., Woltring, H.J. & Dortmans, L.J.M.G. 1988 A least-squares algorithm for the
662 equiform transformation from spatial marker co-ordinates. *Journal of Biomechanics* **21**, 45-54.
663 (doi:https://doi.org/10.1016/0021-9290(88)90190-X).

664 [42] Brainerd, E.L., Baier, D.B., Gatesy, S.M., Hedrick, T.L., Metzger, K.A., Gilbert, S.L. & Crisco, J.J.
665 2010 X-ray reconstruction of moving morphology (XROMM): precision, accuracy and applications in
666 comparative biomechanics research. *Journal of Experimental Zoology Part A: Ecological Genetics and*
667 *Physiology* **313A**, 262-279. (doi:doi:10.1002/jez.589).

668 [43] Semechko, A. 2021 Rigid body parameters of closed surface meshes.

669 [44] Parslew, B., Sivalingam, G. & Crowther, W. 2018 A dynamics and stability framework for avian
670 jumping take-off. *Royal Society Open Science* **5**, 181544. (doi:10.1098/rsos.181544).

671 [45] Daley Monica, A. & Biewener Andrew, A. 2011 Leg muscles that mediate stability: mechanics
672 and control of two distal extensor muscles during obstacle negotiation in the guinea fowl.
673 *Philosophical Transactions of the Royal Society B: Biological Sciences* **366**, 1580-1591.
674 (doi:10.1098/rstb.2010.0338).

675 [46] Allen, V.R., Kambic, R.E., Gatesy, S.M. & Hutchinson, J.R. 2017 Gearing effects of the patella
676 (knee extensor muscle sesamoid) of the helmeted guineafowl during terrestrial locomotion. *Journal*
677 *of Zoology* **303**, 178-187. (doi:doi:10.1111/jzo.12485).

678 [47] Carr, J.A., Ellerby, D.J. & Marsh, R.L. 2011 Function of a large biarticular hip and knee extensor
679 during walking and running in guinea fowl (Numida meleagris). *The Journal of*
680 *Experimental Biology* **214**, 3405. (doi:10.1242/jeb.060335).

681 [48] Trepczynski, A., Kutzner, I., Schwachmeyer, V., Heller, M.O., Pfitzner, T. & Duda, G.N. 2018
682 Impact of antagonistic muscle co-contraction on in vivo knee contact forces. *Journal of*
683 *NeuroEngineering and Rehabilitation* **15**, 101. (doi:10.1186/s12984-018-0434-3).

684 [49] Hutchinson, J.R., Rankin, J., Rubenson, J., Rosenbluth, K.H., Siston, R.A. & Delp, S.L. 2015
685 Musculoskeletal modelling of an ostrich (Struthio camelus) pelvic limb: influence of limb orientation
686 on muscular capacity during locomotion. *Peerj* **3**, 52. (doi:10.7717/peerj.1001).

687 [50] Hutchinson, J.R., Ng-Thow-Hing, V. & Anderson, F.C. 2007 A 3D interactive method for
688 estimating body segmental parameters in animals: Application to the turning and running
689 performance of Tyrannosaurus rex. *Journal of Theoretical Biology* **246**, 660-680.
690 (doi:10.1016/j.jtbi.2007.01.023).

691 [51] Mayr, G. 2016 Variations in the hypotarsus morphology of birds and their evolutionary
692 significance. *Acta Zoologica* **97**, 196-210. (doi:https://doi.org/10.1111/azo.12117).

693 [52] Field, D.J., Bercovici, A., Berv, J.S., Dunn, R., Fastovsky, D.E., Lyson, T.R., Vajda, V. & Gauthier,
694 J.A. 2018 Early Evolution of Modern Birds Structured by Global Forest Collapse at the End-
695 Cretaceous Mass Extinction. *Current Biology*. (doi:https://doi.org/10.1016/j.cub.2018.04.062).

696 [53] !!! INVALID CITATION !!! [3, 49].

697 [54] Ehrig, R.M., Taylor, W.R., Duda, G.N. & Heller, M.O. 2007 A survey of formal methods for
698 determining functional joint axes. *Journal of Biomechanics* **40**, 2150-2157.
699 (doi:https://doi.org/10.1016/j.jbiomech.2006.10.026).

700 [55] Marieswaran, M., Sikidar, A., Goel, A., Joshi, D. & Kalyanasundaram, D. 2018 An extended
701 OpenSim knee model for analysis of strains of connective tissues. *BioMedical Engineering OnLine* **17**,
702 42. (doi:10.1186/s12938-018-0474-8).

703   [56] Brown, N.P., Bertocci, G.E., Cheffer, K.A. & Howland, D.R. 2018 A three dimensional multiplane
704   kinematic model for bilateral hind limb gait analysis in cats. *PLOS ONE* **13**, e0197837.
705   (doi:10.1371/journal.pone.0197837).
706   [57] Kilbourne, B.M., Andrada, E., Fischer, M.S. & Nyakatura, J.A. 2016 Morphology and motion:
707   hindlimb proportions and swing phase kinematics in terrestrially locomoting charadriiform birds. *J
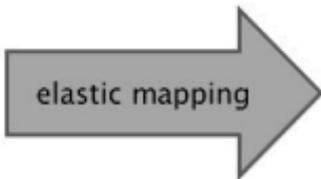708   Exp Biol* **219**, 1405-1416. (doi:10.1242/jeb.124081).

709
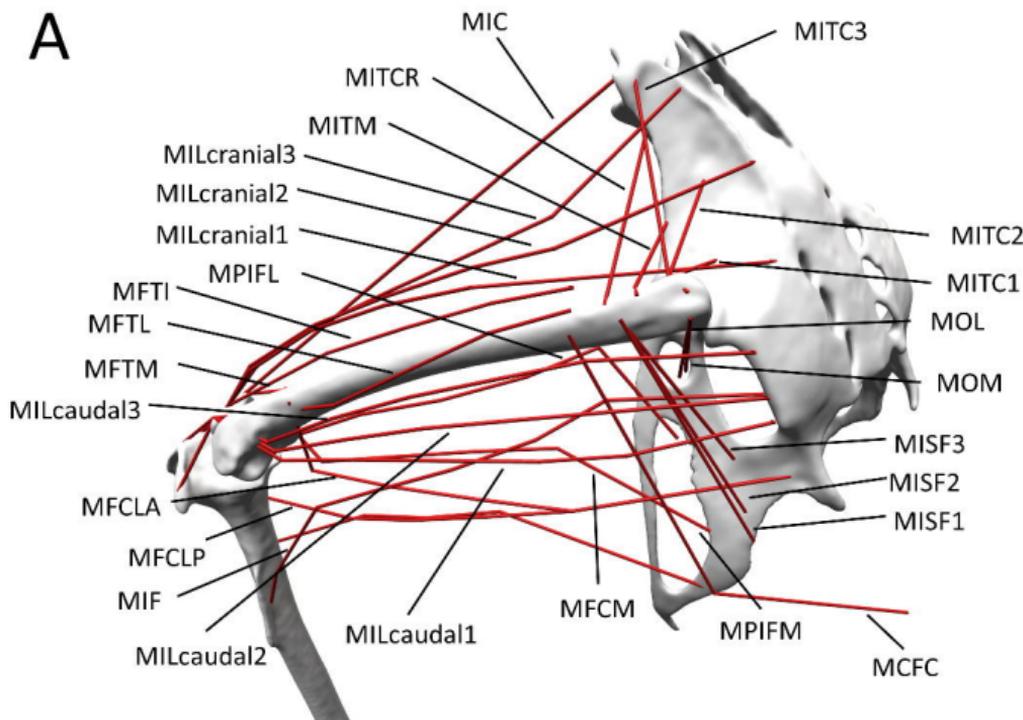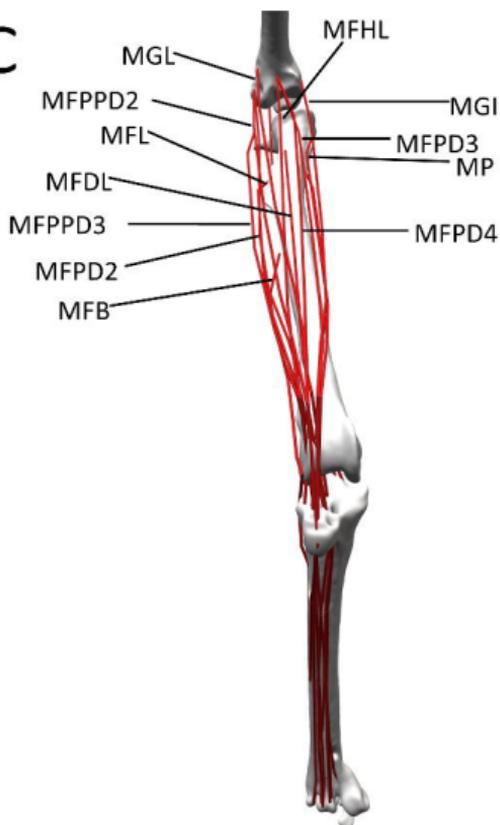
A establish elastic mapping by comparing magpie and zebra finch bone surfaces

magpie bone

zebra finch bone

elastic mapping

B apply elastic mapping to muscle attachment and via point data

magpie bone

zebra finch bone

elastic mapping

pelvis

femur

knee

hip

tibiotarsus

ankle

perch

tarsometatarsus

| T [%] | 0% | 33% | 66% | 100% |